Journal of Power Sources 647 (2025) 237303

Contents lists available at ScienceDirect

Journal of Power Sources

journal homepage: www.elsevier.com/locate/jpowsour

Diagnosis of ionomers degradation in proton-exchange membrane fuel cell

Tangfei Zheng [a,1], Jing Xie [a,1], Ruiqi Zhang [a,1], Guangyao Zhao [a,1], Hua Fan [a], Yong Feng [a,b,c], Shiwen Wang [d], Jian Wang [a,*], Wei Ding [a,**]

[a] Center of Advanced Electrochemical Energy (CAEE), Institute of Advanced Interdisciplinary Studies, State Key Laboratory of Advanced Chemical Power Sources (SKL-ACPS), School of Chemistry and Chemical Engineering, Chongqing University, Chongqing, 400044, China
[b] State Key Laboratory of Advanced Chemical Power Sources Guizhou Meiling Power Sources Co.Ltd., Zunyi, 563003, China
[c] State Key Laboratory of Advanced Chemical Power Sources Guizhou Meiling Power Sources Co.Ltd., Zunyi, Guizhou, 563000, China
[d] Chongqing HiTHIUM Energy Storage Technology Co., Ltd, Chongqing, 404000, China

HIGHLIGHTS

- A new way to identify critical parameters of degraded ionomers.
- The PEMFC performance strongly depends on dry proton accessibility, ECSA, and R_{local}.
- The dynamic decay behavior of ionomer aligns with a first-order exponential decay.

ARTICLE INFO

Keywords:
Degradation
Diagnostic technology
Ionomer
PEMFC

ABSTRACT

The ionomer, a key component in the proton exchange membrane fuel cell (PEMFC), plays a determining role in ions/oxygen transport in the catalytic layer, which dominates the performance of PEMFC. However, the degradation of ionomers within the catalyst layer, including decay behavior and diagnostic states, has rarely been reported, as its decay is usually accompanied by the decay of other components of the catalyst layer, such as the catalyst or interface. Herein, we identified critical parameters of degraded ionomers and established their correlation with PEMFC performance by using an isolated H_2O_2 chemical accelerated stability test (C-AST). The performance of the PEMFC strongly depends on the dry proton accessibility, the electrochemical active surface area, and the oxygen transfer resistance, all of which are greatly affected by the decay of the ionomer during C-AST, especially by the decay of the main chain of ionomer with the breaking of C-F bond. A first-order elementary decay model was constructed by correlating the PEMFC key parameters with the ionomer aging time. This investigation provides a robust basis for understanding the ionomer decay mechanism and informs modifications of ionomer properties to enhance PEMFC durability.

1. Introduction

Polymer electrolyte membrane fuel cells (PEMFCs) have obtained ever-growing interest resulting in significant potential green power source applications [1,2]. Recent advancements in key components and membrane electrode assemblies (MEAs) have significantly enhanced both the activity and stability of PEMFCs [3,4]. Extensive research has focused on determining the lifespans of proton membranes, gas diffusion layers, and catalysts, enabling not only accurate lifespan prediction of PEMFCs but also optimization of their operational efficiency [5–11]. However, the proton ionomer, which facilitates proton transfer and acts as a binder between catalyst particles in the catalytic layer, has received comparatively less attention regarding its longevity. Despite Nafion, produced by DuPont, being the most prevalent and stable ionomer in PEMFCs, its fluoropolymer backbone and sulfonic acid side chains are susceptible to hydrogen peroxide attack over extended operation [12–16]. Particularly, there is pronounced degradation of the ionomer near the anode/membrane interface. Takasaki et al. [17] proposed monitoring ionomer degradation by analyzing decomposition products extracted from fuel cells using solvents, which revealed six degradation

* Corresponding author.
** Corresponding author.
E-mail addresses: wangjian-fc@cqu.edu.cn (J. Wang), dingwei128@cqu.edu.cn (W. Ding).
[1] These authors contributed equally.

https://doi.org/10.1016/j.jpowsour.2025.237303
Received 5 February 2025; Received in revised form 29 April 2025; Accepted 7 May 2025
Available online 14 May 2025

products present after 850 h under open circuit voltage (OCV) conditions and 2800 h under cyclic load testing. By utilizing the impedance variation method, Xie et al. [18] elucidated that ionomer degradation exacerbated catalyst agglomeration in the cathode during the initial 500 h of operation following prolonged testing. In summary, the degradation behavior of ionomers within a fuel cell is complex (Table S1). The ex-situ methods, including AFM, TEM, and XPS, can qualitatively characterize the changes in the morphology, particle size, and surface functional group of the catalytic layer after fuel cell durability testing. On the other hand, in-situ methods such as ion tomography et al. –observed ionomer damage during fuel cell operation. All these approaches point to the occurrence of ionomer degradation within the fuel cell operation. However, the correlation of the decay behavior and diagnostic states of ionomers with PEMFC performance was still unclear, as its decay is usually accompanied by the decay of other components of the catalyst layer in membrane electrode assemblies (MEAs), which are of importance for the development of high stable low Pt loading fuel cells.

Herein, we identified critical parameters of degraded ionomers and established their correlation with PEMFC performance by using an isolated H_2O_2 chemical accelerated stability test (C-AST). In the isolated H_2O_2 chemical accelerated stability test, the decay of the ionomer was accelerated by the Fenton reagent to simulate chemical attacks in the catalyst layer. In order to control the decay rate and conditions, the ionomer was fabricated into a membrane before eroding. The aged ionomer, obtained by dissolving the aged membrane, was then incorporated into a membrane electrode assembly (MEA) for evaluation. Results indicated the morphology of the ionomer was swelled and ruptured from a filamentous structure to small flakes, especially by the decay of the main chain of the ionomer with the breaking of the C-F bond. The relevancy ranking of key parameters for the performance of the PEMFC is the dry proton accessibility, the electrochemical active surface area, and the oxygen transfer resistance, all of which are greatly affected by the decay of the ionomer during C-AST. The dynamic decay behavior of the ionomer aligns with the empirical equation of first-order exponential decay.

2. Experimental

Materials. The main material of study was the D520 Nafion ionomer provided by Dupont. A 30 % peroxide solution and analytical grade $FeCl_2{\cdot}4H_2O$ were obtained from Chongqing Chuandong Chemical Industry Group Co. LTD.

Accelerated durability test. 20 mL DuPont D520 Nafion was cast on a dry glass plate to form a film. The glass plate was placed in an oven at 70 °C for 12 h to remove volatile organic solvents and obtain the film. Clean the ionomer film with ultra-pure water for 3 to 5 times, place it in a beaker and dry it in an oven at 50 °C for 12 h for later use. The dried ionomer film was cut into 3.5*3.5 cm^2, and the cut ionomer film was placed in a certain mass fraction of the Fenton reagent for the accelerated aging experiment. In this experiment, the Fenton reagent is hydrogen peroxide with a mass fraction of 30 %, the catalyst Fe^{2+} is introduced by $FeCl_2$, and the concentration is 5 ppm. After some time, the ionomer film is taken out and washed 3 to 5 times with ultra-pure water to remove the residual Fenton reagent in the film. Then the film is placed in dilute sulfuric acid solution with a mass fraction of 8 % for 24 h to treat the residual metal ions on the surface of the film to achieve H^+ exchange. Then, the film after pickling was washed with ultra-pure water 3 to 5 times to remove the residual dilute sulfuric acid on the surface. Finally, the film after washing was placed in the oven at 50 °C for constant temperature drying for 24 h for reserve. After drying, the dry film quality is weighed, and the average value is measured three times. The dried ionomer film was placed in a round-bottomed flask, and a certain amount of isopropyl alcohol was added to the flask to form an ionomer solution with a mass fraction of 5 %. The flask was placed in a constant temperature oil bath at 70 °C for 24 h and stirred until the ionomer was completely dissolved to prepare the aging ionomer solution.

The test of proton conductivity. The proton conductivity (σ) of ionomer films were measured using Solartron 1260 and Solartron 1287 in combination with a membrane resistance system (MTS-740, Scribner) in a longitudinal way, at different temperatures, testing under a fully hydrated state was done by immersing the sample in DI water with a home-made fixture, and the frequency range was from 1 Hz to 10 MHz. Samples (H^+ form) were cut into 3 cm × 1 cm splines. The experiment was repeated three times for each sample to obtain the average value. σ was determined by the following formula:

$$\sigma = \frac{L}{RS}$$

L is the distance between the electrodes (cm), R is the impedance (Ω), S is the cross-sectional area (cm^2).

IEC measurement. The ion exchange capacity (IEC) of the membrane was determined by acid-base molar titration. The mass W of the dry film was weighed and then placed into a sealed reagent bottle containing saturated sodium chloride solution and stirred for 24 h. Then 1 drops of phenolphthalein solution were added into the beaker, and then 0.1 mol/L NaOH (C_{NaOH}) solution was filled into the basic titer for titration. The volume of consumed NaOH solution was recorded as V_{NaOH}, and the experiment was repeated for three times to take the average value. Calculated as follows:

$$IEC = \frac{V_{NaOH} \times C_{NaOH}}{W}$$

In the formula, C_{NaOH} and V_{NaOH} denote the concentration of NaOH and the volume consumed, respectively, respectively, while W denotes the mass of the dry membranes.

Membrane electrode assembly (MEA) preparation. In this experiment, the homogeneous gas diffusion electrode (GDE) process was used to prepare membrane electrode assembly. The carbon paper from Shanghai Hesen HCP120, the anode and cathode catalyst inks are Pt/C (60 wt %) catalyst and PtRu/C (60 wt %) catalyst from Johnson-Matthey, respectively, and the anode Pt loading is 0.4 mg cm^{-2}. The Pt loading of the cathode was 0.07 mg cm^{-2}. Then it was mixed with 5 wt% ionomer solution and a certain amount of isopropyl alcohol, respectively. The weight of the Nafion ionomer and catalyst in the catalyst ink was 1:4. The fresh Nafion ionomer was selected for the anode, and the aged Nafion ionomer was selected for the cathode. Then, the Nafion 212 film was sandwiched between the carbon paper with the anode and the cathode electrode sprayed with the catalytic layer. The film electrode was prepared by hot pressing at 135 °C and 50 kPa in a hot press for 150 s.

Scanning electron microscopy (SEM). The morphology and structure of the ionomer were analyzed using a scanning electron microscope, images were obtained using a JEOLJSM-7800 facility from Nippon Electronics Corporation, and a coating system was used to cover the sample with a 10 nm Au layer to improve electrical conductivity.

Transmission Electron Microscopy (TEM). The dispersion of catalyst ink was observed by transmission electron microscope and the images were obtained by Thermo Fisher Scientific-Talos F200s test system.

Nuclear magnetic resonance (NMR). After dissolving the sample in deuterated solvent and adding an internal standard, a ^{19}F channel was set on the NMR instrument, and the internal standard was used as the reference calibration chemical shift.

Fourier transform infrared spectroscopy (FT-IR): FT-IR was used to study the structure and properties of the sample. According to the adsorption peak position and corresponding intensity of different characteristic spectral peaks, the functional groups contained in the sample can be analyzed and the chemical structure of the sample can be determined. The FT-IR spectra of the sample were measured by Nicolet iS50 Fourier transform infrared spectrometer for the ionomer and ionomer@catalyst with different aging degrees.

X-ray Photoelectron Spectroscopy (XPS): XPS analysis was conducted using a Kratos XSAM800 instrument equipped with a monochromatic Al X-ray source (Al KR, 1.4866 keV). The XPS analysis chamber pressure was maintained at 10^{-7} Pa or lower during data collection. Each spectrum was constructed by averaging of two scans. During data analysis, the binding energy (BE) of the core level C 1s peak was set at 284.8 eV to compensate for surface-charging effects.

Contact Angle test. The contact Angle measuring instrument used in this experiment is SDC-100 droplet Angle contact Angle measuring instrument of Dongguan Precision Instrument Co., LTD. The carbon paper coated with catalyst ink is tested by the droplet method.

Electrochemical tests in single cells. Scribner 850e fuel cell test system was used to test the performance of the MEAs. When the cell temperature is 80 °C, the back pressure is 0.2 MPa, and the reaction gases are H_2 and O_2, the voltage sweep mode is used to scan from 0.2 V cutoff discharge voltage to open circuit voltage (OCV) until the membrane electrode reaches stability to obtain the polarization curve of the membrane electrode. EIS tests were performed in constant-current mode, frequency range 0.1 Hz–10 kHz, current range 0 A–10 A, and impedance spectra of different current densities were recorded. The proton resistance was conducted in potentiostatic mode, and potentiostatic EIS (PEIS) was measured at 0.6 V between 0.1 Hz and 65 kHz with a sinusoidal potential amplitude of 5 mV. The limiting values of ionic resistance terms relevant to the 45-degree straight line are related to the sum of the ionic resistance (R_{ion}) and electronic resistance (R_{ele}), considering the electron conductivity of supporting carbon elements in the TLM equivalent circuit, $Z = \frac{R_{ion}}{3} + R_{ele}$ [19].

The dry proton accessibility of the cathode was measured by cyclic voltammetry with Scribner 885-HS. When the cell temperature was 80 °C, the back pressure was 0.2 MPa, and the reaction gases were H_2 and N_2, the anode was used as the counter electrode and reference electrode, and the cathode was used as the working electrode. The voltage scanning range was 0.05 V–1.2 V, and the CO dissolution peak of the membrane electrode was measured under dry conditions. Then keep the other conditions unchanged, adjust the cathode RH to 100 %, and then carry out the same steps and the same procedure of scanning to measure the CO dissolution peak of the membrane electrode under wet condition, comparing the CO dissolution peak under dry condition with that under wet condition to obtain the dry proton accessibility of the membrane electrode.

Oxygen local mass transfer impedance R_{other} was obtained by the limiting current method. When the cell temperature is 80 °C, the RH of the anode and the cathode is 60 %, and the reaction gas is H_2 and 1 % O_2, the voltage range is open circuit voltage to 0.05V, and the sweep speed is 5 mV s^{-1}. The constant voltage mode is used to measure the limit current of the membrane electrode under different pressures, and the polarization curve is obtained.

3. Results and discussion

The morphology of the D520 Nafion ionomer was systematically evaluated under varying aging conditions. As depicted in Fig. 1, the pristine ionomer exhibited a filamentous architecture with an average diameter of approximately 30 nm. With escalating concentrations of the Fenton reagent, the filamentous structure progressively swelled and, in some instances, ruptured. This observation suggests that the main and side chains of the polymer molecules were susceptible to attack by potent oxidizing radicals, leading to the disruption of the original morphology during ionomer degradation. The ion exchange capacity (IEC) and proton conductivity, as shown in Fig. S1 and Table S2, decreased with the increase of Fenton reagent concentration. Specifically, the IEC and proton conductivity of the ionomers is down 23.6 % and 16.6 % after the chemical accelerated stability test of 30 % Fenton reagent, respectively. The aged ionomers were also evaluated using FT-

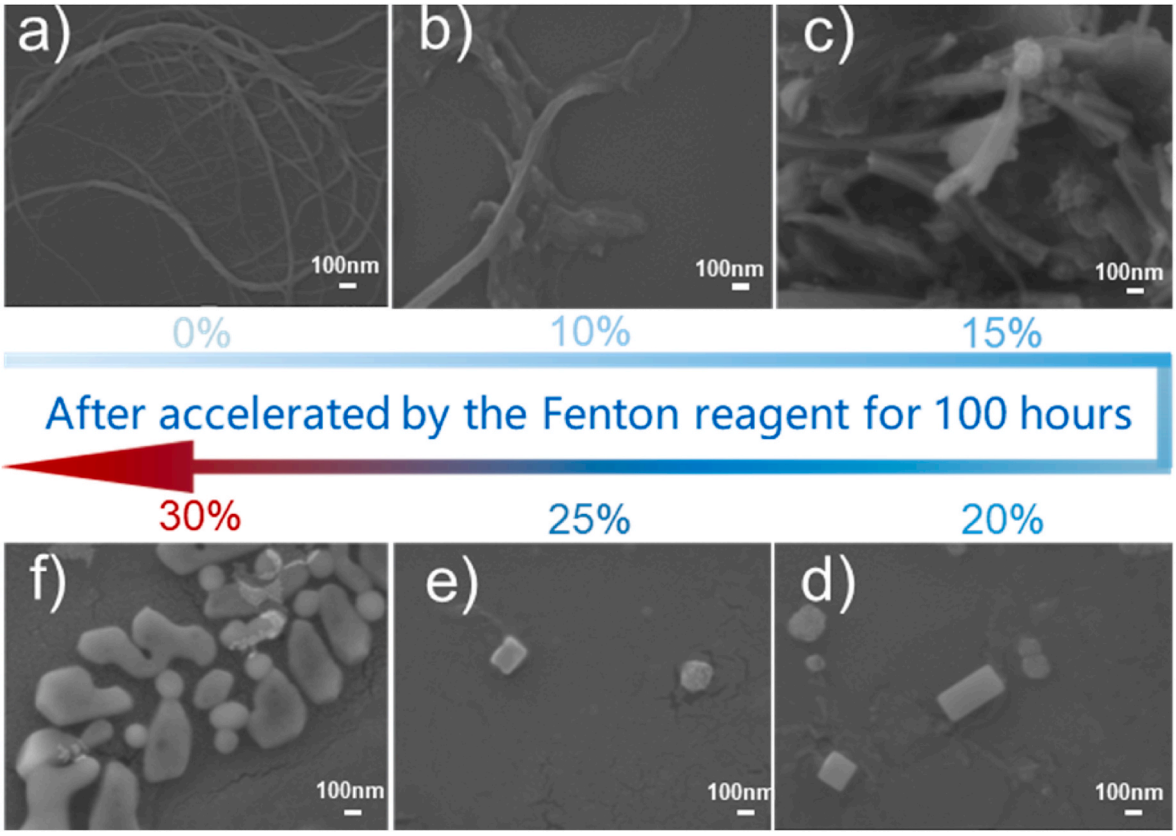

Fig. 1. SEM of DuPont D520 Nafion after aging for 100 h by Fenton reagent of different concentrations: (a) Fresh; (b) 10 % Fenton; (c) 15 % Fenton; (d) 20 % Fenton; (e) 25 % Fenton; (f) 30 % Fenton.

IR. As shown in Fig. S2, the peak intensities of the main groups of ionomers decrease with increasing aging. And the FT-IR spectrum of ionomer-catalyst mixture showed a blue shift from 1048 to 1058 cm^{-1} and increased intensity in the differential spectrum of sulfonic acid group (S-O), demonstrating the loss of sulfonic acid group and weakened ionomer-catalyst interaction (Fig. S2 b-c). Further evidence could be found in the XPS spectrum that showed a negative shift in binding energy of Pt after chemical accelerated stability and the nuclear magnetic resonance (NMR) results that showed the breaking of C-F bonds after chemical accelerated stability test (Fig. 2 and Fig. S3).

To further investigate the performance of PEMFC, the different treatment ionomers were dissolved in the catalyst ink. As shown in Fig. 3, a decline in electrochemical performance was observed with increasing concentrations of the Fenton reagent. Notably, the degradation rate of peak current density or current density at 0.67 V for the aged ionomer reached 67 % following exposure to 30 % Fenton reagent for 100 h, suggesting that the corresponding membrane electrode assembly (MEA) neared the threshold of failure as per DOE criteria. Compared to the polarization curves of MEAs before and after the aging test, it was evident that concentration polarization deteriorated with increasing Fenton reagent concentration, indicating that ionomer degradation adversely affects the mass transfer of reactants. The total resistance (R_{Total}) and the mass transfer resistance (R_{mt}) of fresh MEA increased by nearly 4 times after aging by 30 % Fenton reagent for 100 h. This finding indicates that the dispersion of the ionomer and the three-phase interface area within the catalytic layer deteriorates, leading to impaired electron and ion conductivity, thereby obstructing mass transfer channels (Fig. S4 and Table S3).

To elucidate the impact of ionomer degradation, an oxygen concentration of 1 % was employed to assess local oxygen mass transfer resistance via the limiting current method (Fig. S5–6). As Fig. S7 shown, the local oxygen mass transfer resistance of MEAs constructed with aged D520 Nafion ionomer increased with higher Fenton reagent content, indicating that the degraded ionomer impeded oxygen permeability. The results indicate that the local oxygen mass transfer resistance of MEAs constructed with aged D520 Nafion ionomer increased with Fenton reagent content; Moreover, the limiting current density values decrease significantly with ionomer aging. Two possible reasons are responsible for these observations: i) the serious decay of proton conductivity of ionomer as the break of main chains, and ii) the morphology subsidization of ionomer that increases the Knudsen resistance. Additionally, catalyst layers fabricated with aged ionomers were evaluated through water contact angle measurements, as shown in Fig. S8, where the water contact angle decreased with increased Fenton reagent content, suggesting enhanced hydrophilicity of the catalyst layer. To discern the interface between the catalyst and ionomer, as shown in Fig. S9, catalyst ink containing aged ionomer exhibited more pronounced agglomeration than that with fresh ionomer. Consequently, the three-phase interface within the catalyst layer was altered by the aged ionomer, significantly affecting the reactants' mass transfer.

To evaluate the ionomer distribution and the coverage over the catalyst and to elucidate the relationship between the ionomer and the three-phase interface within the catalytic layer, dry proton accessibility was quantified using electrochemical active surface area (ECSA) measurements via CO stripping experiments conducted at 20 % RH and 100 % RH (Fig. 4). Worthy, the onset potential of CO stripping curves increased with content of Fenton reagent at 20 % RH, demonstrating that the interface reaction region constructed by aged ionomer was disadvantaged to transport of proton and reactants. As shown in Fig. 5, the ECSA via CO stripping at 100 % RH was reduced by 71.6 % of the fresh one, attributed to low ionomer coverage, diminished proton conduction, and its altered interaction with Pt particles post-aging. The dry proton accessibility decreased by 42.2 % of the fresh one with increasing Fenton reagent content, indicating that the interface between ionomer and Pt deteriorated. Similarly, the local oxygen transport resistance (R_{other}) had increased by 3.4 times on the basis of fresh one, demonstrating that the destroyed ionomer hindered the transport of oxygen. Furthermore, the correlation between the decay rate of the performance of PEMFCs and key parameters was constructed. The specific correlations are sorted as follows the dry proton accessibility, the ECSA via CO stripping at 100 % RH, and local oxygen transfer resistance. The PEM fuel cells fabricated by different degraded ionomers were analyzed by the Nyquist plots with H_2/N_2. As shown in Fig. S10, the proton transport resistance (R_{ion}) within the catalyst layers increased with the Fenton reagent concentration. The R_{ion} of the aged ionomer is 6.4 times more than that of fresh ionomer, indicating that the proton transport paths of the ionomer are mostly destroyed after the chemical accelerated stability test. These results are consistent with the dry proton accessibility decay trend detected by using the electrochemical surface area (ECSA), which showed only 28.4 % of ECSA remained and dry proton accessibility decreased by 42.2 % after C-AST. Therefore, the decayed proton conductivity limited the proton supply into the active sites, leading to the lowered ECSA and dry proton accessibility, which greatly decreased the reactivity of the catalyst. The altered morphology of the ionomer, however, blocks the pores where the aged ionomer is present, as the morphology of the ionomer changes from a chain to a particle after C-AST.

Thus, further identification of progressively degraded ionomers was conducted using a 20 % Fenton reagent. As illustrated in Fig. 6, the performance of MEAs declined with aging time, with over 70 % performance loss compared to fresh ones after a 250-h aging test, indicating that the MEA met the inactivation standard based on DOE protocol. Specifically, the ECSA and dry proton accessibility significantly decreased (Fig. 5), while resistance markedly increased (Fig. S11, Table S4), indicating substantial damage to reactant mass transfer pathways within the three-phase interface region of the catalyst layer following prolonged continuous aging. The primary cause is elucidated by XPS results, which show that the F atom ratio decreased from 55.13 % to 45.74 %, and the S atom ratio decreased from 1.71 % to 1.23 %, indicating that the ionomer backbones and side chains were damaged by

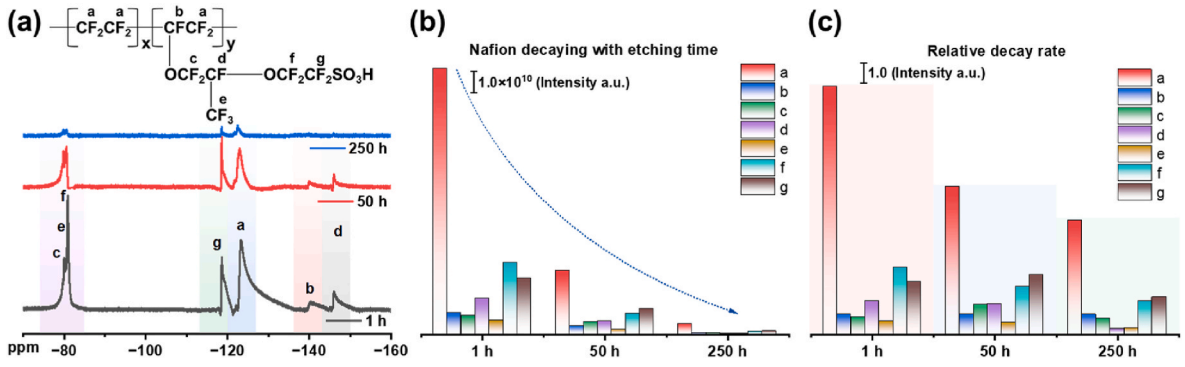

Fig. 2. Nuclear magnetic resonance of ionomer with different aging times.

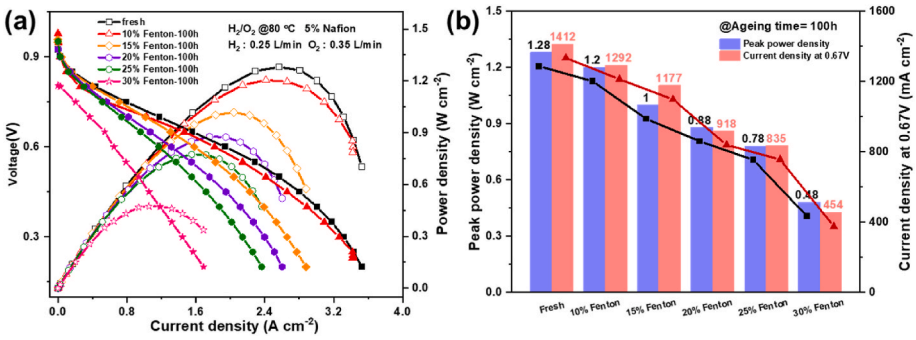

Fig. 3. MEA prepared by aging DuPont D520 Nafion ionomer in Fenton reagent of different concentrations for 100 h: (a) H_2/O_2 polarization curve and corresponding power density curve; (b) Peak power density and current density change at 0.67V

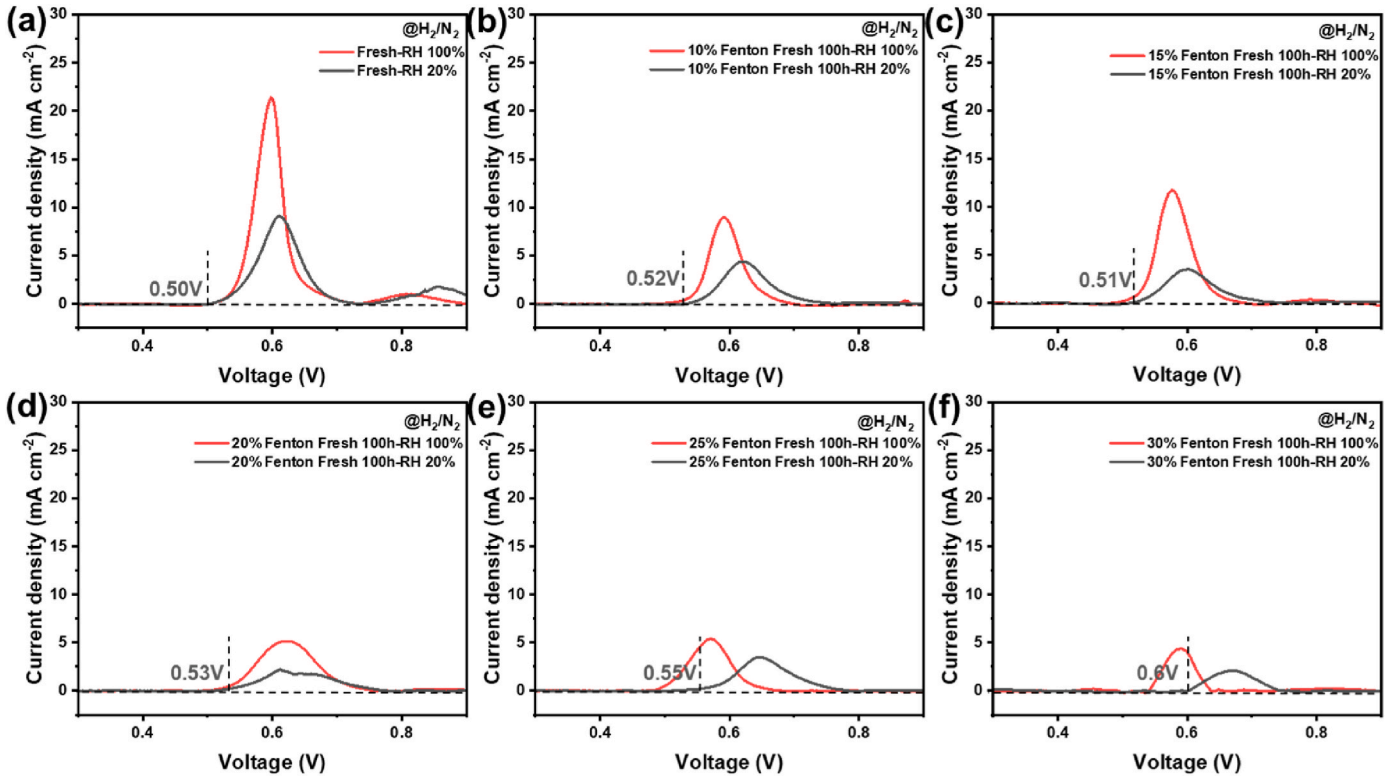

Fig. 4. CO dissolution diagram of MEA prepared by DuPont D520 Nafion ionomer after aging for 100h in Fenton reagent of different concentrations under different humidity:(a) Fresh; (b) 10 % Fenton; (c) 15 % Fenton; (d) 20 % Fenton; (e) 25 % Fenton; (f) 30 % Fenton.

the Fenton reagent (Fig. S12, Table S5).

Furthermore, the relationship between key parameters (the dry proton accessibility, ECSA via 100 % RH, oxygen transfer resistance) of PEMFC and the aging time of ionomer was established, which was consistent with the first-order elementary function after fitting. The equation follows:

$$y = Ae^{\frac{-x}{B}} + C$$

Where y denotes the degradation rate of ionomer; A represents the amount related to aging time in the aging or degradation process of ionomer, such as degree of catalyst coverage, and electrical conductivity. B represents the environmental influences on the ionomer's aging or degradation process, including Fenton reagent concentration, metal ion content, and humidity pressure. C represents the time-independent amount in the aging degradation process, such as the glass transition temperature.

As Fig. 7a shown, the dry proton accessibility and ECSA via 100 % RH decreased with aging time, which was consistent with the decay trend of current density @0.67V and peak power density (Fig. 7c). In contrast, the R_{Total} and R_{mt}, increased along with aging time, indicating the mass transfer paths of reactants were impeded (Fig. 7b). The results indicate that as the rate of parameter change increases, reflecting the extent of film degradation, the more pronounced the degradation of battery performance becomes. Thus, a predictive life model for the ionomer can be constructed using key parameters—dry proton accessibility, ECSA at 100 % RH, and resistance—alongside PEMFC performance metrics. This model offers a robust framework for elucidating ionomer decay mechanisms and informing modifications to ionomer properties.

4. Conclusion

This work provides a new way to identify critical parameters of degraded ionomers and establish their correlation with PEMFC

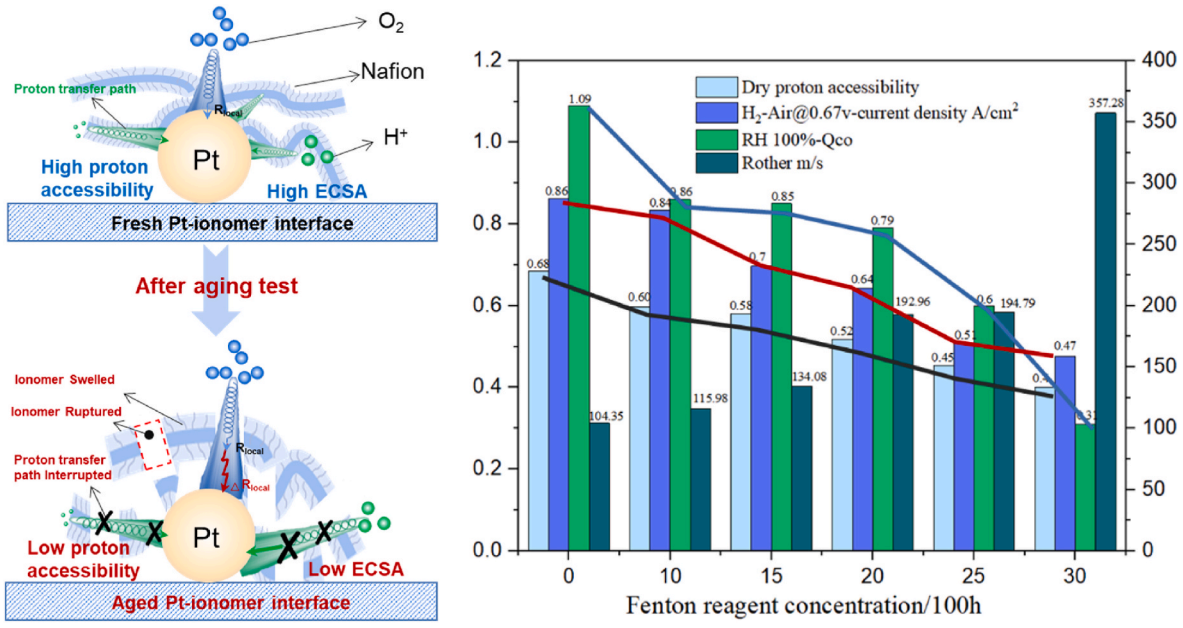

Fig. 5. The key parameters of MEA prepared by DuPont D520 Nafion ionomer after aging for 100 h with different content of Fenton reagent.

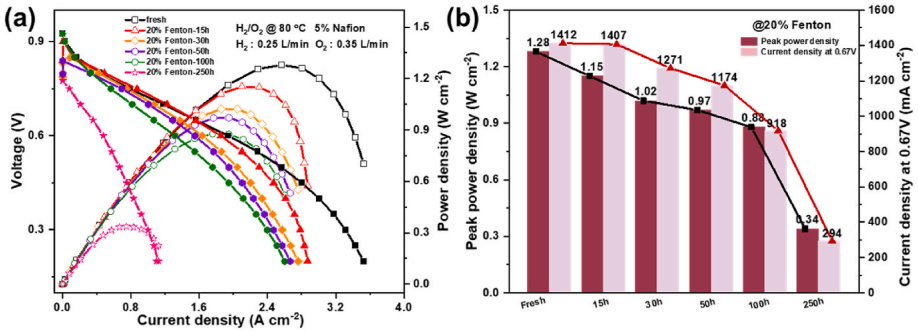

Fig. 6. MEA prepared by aging of DuPont D520 Nafion ionomer in 20 % Fenton reagent for different time: (a) H_2/O_2 polarization curve and corresponding power density curve; (b) Peak power density and current density change at 0.67V

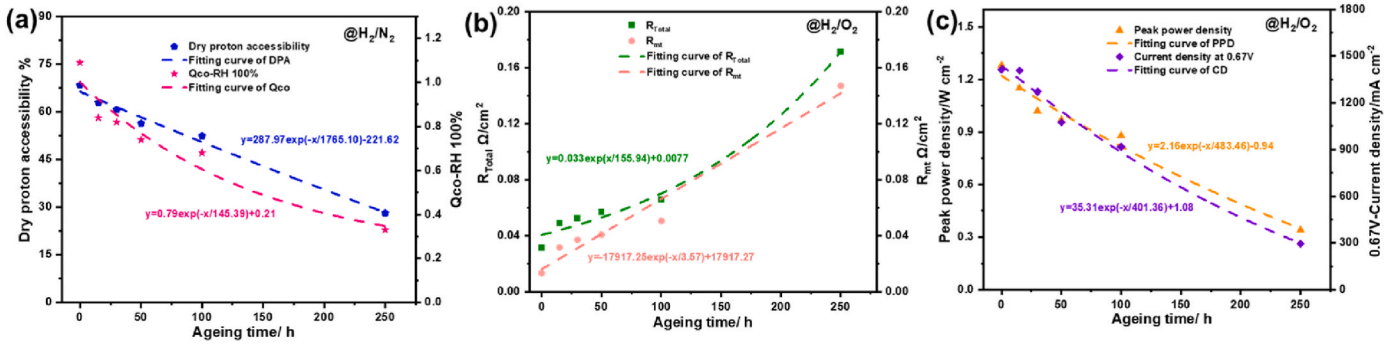

Fig. 7. The fitting curve of the key parameters of the MEA prepared by DuPont D520 Nafion ionomer after aging in 20 % Fenton system for different time varies with aging time: (a) dry proton accessibility and CO dissolution peak area (100 % RH) (b) R_{Total} and R_{mt};(c) Peak power density and current density@0.67V

performance by using an isolated H_2O_2 chemical accelerated stability test (C-AST). The morphology of the ionomer was swelled and ruptured from a filamentous structure to small flakes after C-AST, especially by the decay of the main chain of ionomer with the breaking of the C-F bond. The correlation between the decay rate of the performance of PEMFCs and key parameters was constructed. The specific correlations are sorted as follows the dry proton accessibility, the ECSA via CO stripping at 100 % RH, and local oxygen transfer resistance. Also, a first-order elementary decay model was constructed by correlating the PEMFC key parameters with the ionomer aging time. This investigation provides a robust basis for understanding the ionomer decay mechanism and informs modifications of ionomer properties to enhance PEMFC durability. Ionomer networks not only provide proton conduction pathways but also stabilize electrode microstructure, enhance electronic

connectivity, and regulate reaction kinetics through interfacial interactions, enabling robust and highly efficient gas-liquid-solid three-phase interfaces for modern electrochemical devices, such as fuel cells, electrolyzers, and flow batteries, etc [20–25]. These electrochemical devices rely on the effective synergy of these functions to achieve efficient energy conversion. The ionomer degradation is a key challenge across these technologies, which lies in reactive oxygen species (ROS)-induced ionomer degradation. For instance, during oxygen evolution reactions (OER) at high anode potentials (>1.5 V vs. RHE), parasitic two-electron transfer pathways generate H_2O_2 intermediates. Subsequent Fenton-type reactions between H_2O_2 and trace metal ions (e.g., Fe^{2+}) produce hydroxyl radicals (•OH), which attack ionomer chains through radical oxidation mechanisms [26,27]. These by-products not only affect the chemical stability of the ionomer but may also lead to its degradation, significantly reducing proton conductivity and ionic transport properties. Therefore, conducting in-depth research on ionomers and their behavior in reactive environments is not only critical for advancing fuel cell technology but also provides valuable theoretical foundations and practical guidance for designing future novel energy conversion devices.

CRediT authorship contribution statement

Tangfei Zheng: Data curation. **Jing Xie:** Data curation. **Ruiqi Zhang:** Data curation. **Guangyao Zhao:** Data curation. **Hua Fan:** Data curation. **Yong Feng:** Data curation. **Shiwen Wang:** Data curation. **Jian Wang:** Writing – original draft. **Wei Ding:** Writing – review & editing.

Declaration of competing interest

The authors declare that they have no known competing financial interests or personal relationships that could have appeared to influence the work reported in this paper.

Acknowledgments

This study was financially supported by the National Key R&D Program of China (2021YFA1502000), the National Natural Science Foundation of China (22022502, 22208034, and 22179012), the Natural Science Foundation of Chongqing, China (CSTB2023NSCQ-LZX0084).

Appendix A. Supplementary data

Supplementary data to this article can be found online at https://doi.org/10.1016/j.jpowsour.2025.237303.

Data availability

The data that support the findings of this study are available from the corresponding author upon reasonable request.

References

[1] M.K. Debe, Electrocatalyst approaches and challenges for automotive fuel cells, Nature 486 (2012) 43–51.
[2] Y. Nie, L. Li, Z. Wei, Recent advancements in Pt and Pt-free catalysts for oxygen reduction reaction, Chem. Soc. Rev. 44 (2015) 2168–2201.
[3] C. Lee, W.J.M. Kort-Kamp, H. Yu, D.A. Cullen, B.M. Patterson, T.A. Arman, S. Komini Babu, R. Mukundan, R.L. Borup, J.S. Spendelow, Grooved electrodes for high-power-density fuel cells, Nat. Energy 8 (2023) 685–694.
[4] J. Wang, G. Wu, W. Wang, W. Xuan, J. Jiang, J. Wang, L. Li, W.-F. Lin, W. Ding, Z. Wei, A neural-network-like catalyst structure for the oxygen reduction reaction: carbon nanotube bridged hollow PtCo alloy nanoparticles in a MOF-Like matrix for energy technologies, J. Mater. Chem. A 7 (2019) 19786–19792.
[5] Y. Feng, J. Xie, G. Zhao, X. Li, J. Wang, W. Ding, Z. Wei, Degradation study and diagnostic technology for nafion membrane, J. Power Sources 613 (2024) 234880.
[6] J.M. Morgan, R. Datta, Understanding the gas diffusion layer in proton exchange membrane fuel cells. I. How its structural characteristics affect diffusion and performance, J. Power Sources 251 (2014) 269–278.
[7] R.B. Ferreira, D.S. Falcão, V.B. Oliveira, A.M.F.R. Pinto, Experimental study on the membrane electrode assembly of a proton exchange membrane fuel cell: effects of microporous layer, membrane thickness and gas diffusion layer hydrophobic treatment, Electrochim. Acta 224 (2017) 337–345.
[8] P. Ren, P. Pei, Y. Li, Z. Wu, D. Chen, S. Huang, Degradation mechanisms of proton exchange membrane fuel cell under typical automotive operating conditions, Prog. Energy Combust. Sci. 80 (2020) 100859.
[9] M. Tang, S. Zhang, S. Chen, Pt utilization in proton exchange membrane fuel cells: structure impacting factors and mechanistic insights, Chem. Soc. Rev. 51 (2022) 1529–1546.
[10] M.A. Abdelkareem, K. Elsaid, T. Wilberforce, M. Kamil, E.T. Sayed, A. Olabi, Environmental aspects of fuel cells: a review, Sci. Total Environ. 752 (2021) 141803.
[11] X. Gui, A.A. Auer, Electronic structure simulations of the platinum/support/ionomer interface in proton exchange membrane fuel cells, Fuel Cells 25 (2024) e202400117.
[12] S. Lee, J. Nam, J. Ahn, S. Yoon, S.C. Jeong, H. Ju, C.H. Lee, Perfluorinated sulfonic acid ionomer degradation after a combined chemical and mechanical accelerated stress test to evaluate membrane durability for polymer electrolyte fuel cells, Int. J. Hydrogen Energy 96 (2024) 333–342.
[13] C. Yue, W. Zheng, Y. Lian, J. Kang, S. Chen, X. Dong, B. Li, C. Zhang, P. Ming, Decomposition on the degradation mechanism of the cathode catalyst layer under 1000 h of on-road heavy-duty transportation, J. Energy Storage 104 (2024).
[14] J. Miyake, R. Taki, T. Mochizuki, R. Shimizu, R. Akiyama, M. Uchida, K. Miyatake, Design of flexible polyphenylene proton-conducting membrane for next-generation fuel cells, Sci. Adv. 3 (2017) eaao0476.
[15] M. Wang, S. Zhang, H. Wang, E. Sun, Y. Liu, M. Wu, D.-J. Liu, Z. Li, Regulating catalyst and ionomer interactions to promote oxygen transport in fuel cells, Appl. Catal., B: Environ. Energy 365 (2025).
[16] P. Qi, Z. Wu, J. Mou, D. Wu, Y. Gu, M. Xu, Z. Li, Y. Luo, A review of water management in proton exchange membrane fuel cell systems, Sustain. Energy Fuels 9 (2025) 72–97.
[17] M. Takasaki, K. Kimura, K. Kawaguchi, A. Abe, G. Katagiri, Structural analysis of a perfluorosulfonate ionomer in solution by 19F and 13C NMR, Macromolecules 38 (2005) 6031–6037.
[18] M. Yaldagard, M. Jahanshahi, N. Seghatoleslami, Carbonaceous nanostructured support materials for low temperature fuel cell electrocatalysts—A review, World J. Nano Sci. Eng. 3 (2013) 121–153.
[19] J. Kwon, P. Choi, K. Eom, A comparison study on the carbon corrosion reaction under saturated and low relative humidity conditions via transmission line model-based electrochemical impedance analysis, J. Electrochem. Soc. 168 (2021) 064515.
[20] Y. Liu, H. Ding, D. Si, J. Peng, J. Zhang, A review of proton exchange membrane fuel cell catalyst layer by electrospinning, J. Electrochem. 24 (2018) 639–654.
[21] F. Chen, Z. Xie, M. Li, S. Chen, W. Ding, L. Li, J. Li, Z. Wei, High-performance oxygen reduction catalysts for fuel cells, J. Electrochem. 30 (2024) 2314007.
[22] L. Xia, H. Liu, L. Liu, Z. Tan, Recent progress in organic redox flow batteries, J. Electrochem. 24 (2018) 466–487.
[23] J. Li, Y. Yao, L. An, S. Wu, N. Zhang, J. Jin, R. Wang, P. Xi, Regulation of perovskite oxides composition for the efficient electrocatalytic reactions, Smart Molecules 1 (2023) e20220005.
[24] Q. He, D. Lin, D. Yin, C. Yang, D. Chen, X. Feng, Propene epoxidation with molecular oxygen: advancements from nanoparticle to single-atom catalysts, Smart Molecules 2 (2024) e20240025.
[25] Y. Feng, J. Xie, G. Zhao, X. Li, J. Wang, W. Ding, Z. Wei, Degradation study and diagnostic technology for nafion membrane, J. Power Sources 613 (2024) 234880.
[26] T. Zheng, M. Ou, S. Xu, X. Mao, S. Wang, Q. He, Recent progress of bifunctional electrocatalysts for oxygen electrodes in unitized regenerative fuel cell, J. Electrochem. 29 (2023) 2205301.
[27] M. Ding, W. Jiang, T. Yu, X. Zhuo, X. Qin, S. Yin, Electronically modulated FeNi composite by CeO_2 porous nanosheets for water splitting at large current density, J. Electrochem. (29) (2023) 2208121.